*Remote Sens.* **2014**, *6*, 421-442; doi:10.3390/rs6010421

OPEN ACCESS

*remote sensing*

**ISSN 2072-4292**

www.mdpi.com/journal/remotesensing

*Article*

# Improved Accuracy of Chlorophyll-a Concentration Estimates from MODIS Imagery Using a Two-Band Ratio Algorithm and Geostatistics: As Applied to the Monitoring of Eutrophication Processes over Tien Yen Bay (Northern Vietnam)

**Nguyen Thi Thu Ha [1,*], Katsuaki Koike [2] and Mai Trong Nhuan [1]**

[1] Faculty of Geology, VNU University of Science, Vietnam National University, Hanoi 334, Nguyen Trai, Thanh Xuan, Hanoi 10000, Vietnam; E-Mail: nhuanmt@vnu.edu.vn

[2] Department of Urban Management, Graduate School of Engineering, Kyoto University, Katsura C1-2-215, Kyoto 615-8540, Japan; E-Mail: koike.katsuaki.5x@kyoto-u.ac.jp

* Author to whom correspondence should be addressed; E-Mail: hantt_kdc@vnu.edu.vn; Tel.: +84-4-3558-7060; Fax: +84-4-3557-3336.

*Received: 24 October 2013; in revised form: 11 December 2013 / Accepted: 20 December 2013 / Published: 30 December 2013*

---

**Abstract:** Sea eutrophication is a natural process of water enrichment caused by increased nutrient loading that severely affects coastal ecosystems by decreasing water quality. The degree of eutrophication can be assessed by chlorophyll-a concentration. This study aims to develop a remote sensing method suitable for estimating chlorophyll-a concentrations in tropical coastal waters with abundant phytoplankton using Moderate Resolution Imaging Spectroradiometer (MODIS)/Terra imagery and to improve the spatial resolution of MODIS/Terra-based estimation from 1 km to 100 m by geostatistics. A model based on the ratio of green and blue band reflectance (rGBr) is proposed considering the bio-optical property of chlorophyll-a. Tien Yen Bay in northern Vietnam, a typical phytoplankton-rich coastal area, was selected as a case study site. The superiority of rGBr over two existing representative models, based on the blue-green band ratio and the red-near infrared band ratio, was demonstrated by a high correlation of the estimated chlorophyll-a concentrations at 40 sites with values measured *in situ*. Ordinary kriging was then shown to be highly capable of predicting the concentration for regions of the image covered by clouds and, thus, without sea surface data. Resultant space-time maps of concentrations over a year clarified that Tien Yen Bay is characterized by natural eutrophic waters, because the average of chlorophyll-a concentrations exceeded 10 mg/m$^3$ in the summer. The temporal changes of chlorophyll-a concentrations were consistent with average monthly air

temperatures and precipitation. Consequently, a combination of rGBr and ordinary kriging can effectively monitor water quality in tropical shallow waters.

**Keywords:** bio-optical properties; water quality; estimation algorithm; phytoplankton; ordinary kriging

## 1. Introduction

Chlorophyll-a (Chl-a) concentration is an effective measure of the trophic state of sea and land waters, because it is related strongly to aquatic phytoplankton abundance and biomass. Estimating Chl-a concentration is one of the most traditional and significant applications of remote sensing for evaluating aquatic ecosystems and monitoring eutrophication [1–5]. Recently, satellite imagery with high spectral resolution spanning the visible to thermal-infrared bands has become available for such estimations. The main targets of substantive case studies using such imagery are environmental assessments of ocean waters [6–9], open coastal and estuarine waters [10–15] and inland lakes [16–19]. In addition to these waters, eutrophication in coastal waters, shallow coastal bays and lagoons has been a notable issue threatening coastal ecosystems all over the world [20]. Despite the importance of Chl-a monitoring in such coastal areas by remote sensing, such applications have been limited, and the most suitable methods for estimating Chl-a concentrations from satellite imagery have not yet been identified. This lack of information is the result of several factors, including the difficulties associated with making atmospheric corrections and the influences of detritus and dissolved organic matter on water optical properties that may not co-vary with phytoplankton [21].

Based on the above conditions, this study aims to identify a suitable method for the estimation using representative satellite imagery, like the Moderate Resolution Imaging Spectroradiometer Terra (MODIS/Terra: MODIS in short hereinafter). The physical relationship between the Chl-a concentration and reflectance spectra of the MODIS bands, but not an empirical relationship, has been considered for the estimation. The MODIS imagery gives the best fit for Chl-a monitoring owing to the advantages of short revisit periods for the same scene (nearly every day) and the wide swath of the satellite [22]. These advantages also make the monitoring of coastal waters by MODIS more convenient in data collection and in comparisons of eutrophication conditions over the world.

Tien Yen Bay in northern Vietnam was selected for the present study, because it is a typical closed and shallow coastal water body that contains a rich and diverse aquatic ecosystem, but one that has a high risk of eutrophication and water-quality degradation. To improve the spatial resolution of Chl-a concentration mapping through MODIS imagery (1 km), a geostatistical technique was adopted as a post-image process. Two common atmospheric correction procedures were compared also to identify the best method to be used with such a MODIS application for the monitoring of Tien Yen Bay waters under tropical weather conditions.

## 2. Materials

### *2.1. Features of the Study Area*

Tien Yen Bay, adjacent to both Vietnam and China, covers an area of approximately 400 km$^2$ and is connected to the South China Sea by five channels (Figure 1). The most remarkable feature of the bay is its shallowness: the sea depth generally ranges from 2 to 5 m; although it becomes deeper in the connecting channels, the maximum depth is still only 20 m. There are five short local rivers that usually transport small quantities of freshwater (the average water discharges of Tien Yen River and Ha Coi River are 22.1 and 7.4 m$^3$/s, respectively) and sediments into the bay. The sediment quantity decreases further in the dry season to 4 mg/L of the total suspended solids. Therefore, the physical and aquatic environment of the bay is a typical closed sea environment, which is influenced mainly by oceanographic factors, such as tide, waves and near-shore currents.

**Figure 1.** Location of Tien Yen Bay in northern Vietnam and the positions of 40 sampling points for measuring Chl-a concentrations.

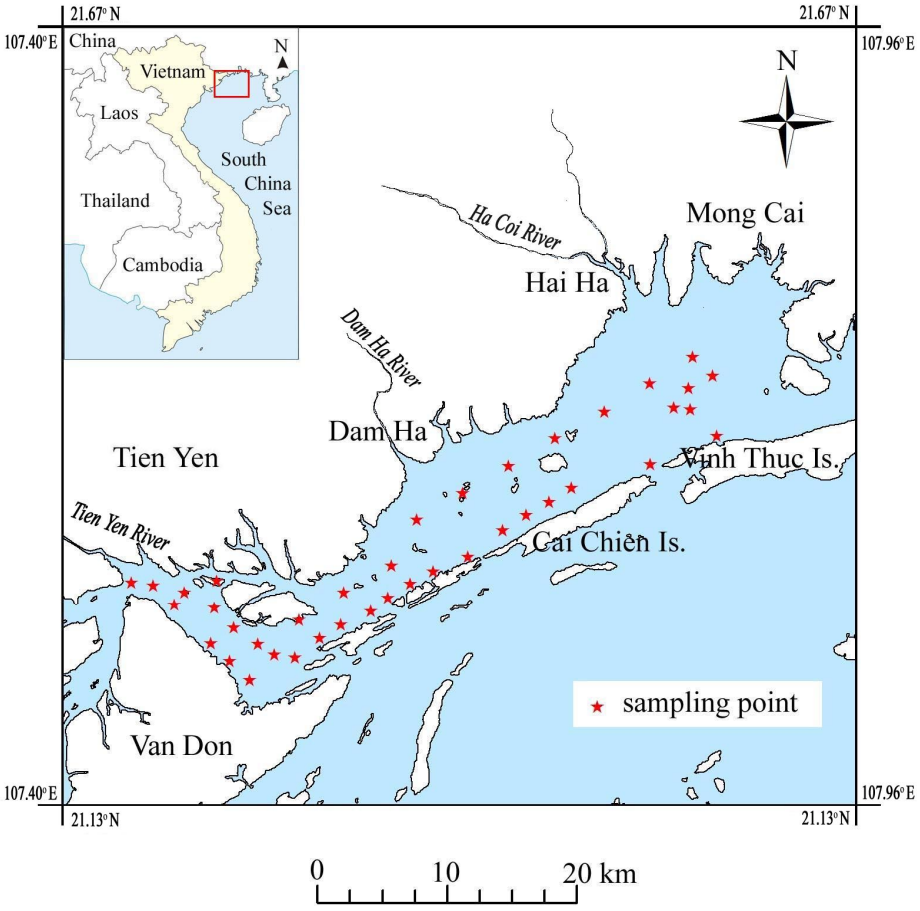


According to the Vietnam Environmental Protection Agency [23], Tien Yen Bay is a nationally significant site of biodiversity, because of the occurrence of 69 species of phytoplankton, 58 species of zooplankton, 33 species of seaweed and four species of seagrass that have been identified in the area [24]. The bay waters encompass a high density of phytoplankton ranging from 6,318 cells/L (dry

season) to 7,352 cells/L (rainy season) on average. The maximum density was recorded as 70,810 cells/L in the rainy season [25]. The most abundant phytoplankton is Bacillariophyta (162 species), which occupies 86% of the total species, and Chlorophyta (12 species), Cyanophyta (8 species) and Pyrrophyta (6 species) follow it in descending order [25]. Therefore, eutrophication may occur and threaten aquatic life in the bay, particularly in the rainy season (June to October). To observe this possibility and to preserve aquatic health, monitoring of water quality in terms of the water trophic state is indispensable. This state can be assessed primarily by Chl-a concentration. Satellite remote sensing, in particular using MODIS imagery with its above-mentioned advantages, is the most suitable procedure for this purpose.

### *2.2. Collection of Sample Data*

Samples of Chl-a concentrations in Tien Yen Bay were collected at 40 locations using a speed-boat on 6 July 2010, with a Global Positioning System (GPS) receiver used to locate the points shown in Figure 1. These points were selected to representatively cover the whole bay. The samples were taken at a depth of 50 cm using a Van Dorn water sampler, preserved in one liter cleaned dark-color bottles, and then refrigerated.

In the laboratory, the water samples were filtered by a pre-washed 47 mm glass fiber filter and then extracted into 90% acetone. The Chl-a concentrations in the extracts were determined spectrophotometrically using a Labomed UV-Vis RS model UV-2502 spectrometer with a 2 nm spectral bandwidth and optically matched 13 mm diameter cuvettes following the standard method of the American Public Health Association [26]. Table 2 in Section 4.2 below includes descriptive statistics of the resultant 40 concentration data, which indicates that the Tien Yen Bay waters have a wide variation (8.4 mg/m$^3$ range), and most data (80%) exceed 10 mg/m$^3$.

The turbidity of the bay waters was also *in situ* measured on 6 July 2010 and ranged from 6 to 15 NTU at the 40 survey sites. The turbidity of 10 NTU approximately corresponds to the 2-m Secchi disk depth [27]. Because the Secchi disk depths are mostly shallower than the water depths of the 40 sites based on the bathymetric map [28], the effect of the bottom reflected radiance is negligible.

### *2.3. MODIS Image Data*

The Terra spacecraft passes over Tien Yen Bay at about 3:20 GMT (10:20 local time) each day. This time is suitable for the acquisition of satellite imagery to compare with *in situ* water quality. MODIS level 1B image data acquired on the same date as the water sampling (6 July 2010), which were calibrated at-aperture radiances for the 36 bands and geo-located for WSG-84 N48 of the UTM system, were used to estimate Chl-a concentrations.

The atmospheric correction of MODIS image data is a necessary part of pre-processing, because the contributions of radiant energy from the atmosphere and from specular reflections at the sea surface must be corrected for extracting the radiant energy from the water body only. The dark-object subtraction (DOS), a histogram minimum method proposed by Chavez [29], was compared with the Quick Atmospheric Correction (QUAC) that is a VNIR-SWIR atmospheric correction method [30] in this study. The DOS was demonstrated as the most effective method for monitoring water quality using visible bands [31,32], while QUAC showed accurate performance for infrared spectral

bands [30]. Ha and Koike [33] also identified that DOS was a more suitable atmospheric correction method for the MODIS image data of Tien Yen Bay than the near-infrared atmospheric correction and Fast Line-of-sight Atmospheric Analysis of Hyperspectral cubes (FLAASH).

## 3. Methods for Estimating Chl-a Concentration

### *3.1. Review of Estimation Algorithms*

Light is absorbed by algal pigments, but scattered by algal cells and non-algal particles. This phenomenon is used in most existing estimation algorithms for Chl-a concentration from optical satellite image data [34], which emphasize the difference between the absorption and scattering by a ratio of reflectances at two wavelength bands or in two certain wavelength ranges. The algorithms can be classified into two groups, depending on the wavelengths used in the ratio. The first uses a ratio of reflectance in the wavelength range between 440 and 510 nm in which Chl-a and carotenoid strongly absorb light and another reflectance in the minimum green pigment region between 550 and 555 nm [21,35]. The second uses a ratio of reflectance in the near-infrared (NIR) region between 685 and 710 nm, in which the water and pigment absorption and the chlorophyll fluorescence have a minimum correlation, and another reflectance in the red chlorophyll absorption band between 670 and 675 nm [4,36].

A representative algorithm for the first group is the blue-green band ratio, which was proposed first by Morel and Prieur [21] for discriminating ocean color. This simple ratio has a robust and sensitive relationship to the Chl-a concentration in ocean waters, but is known to be less sensitive for the 30 mg/m$^3$ or more of Chl-a [4]. The algorithm has been improved in order to make it applicable to coastal waters [7–9,35,37,38]. OC3M developed by O'Reilly *et al.* [9] is the most widely used algorithm of such improvement for estimating global Chl-a concentrations, which is formulated as:

$$C_{Chla} = 10^{a_0+a_1\phi+a_2\phi^2+a_3\phi^3+a_4\phi^4} \quad (1)$$

where $C_{Chla}$ is the Chl-a (mg/m$^3$) concentration, $\phi = \log\{\max[R_{rs}(443):R_{rs}(488)]/R_{rs}(551)\}$, $R_{rs}(\lambda)$ is reflectance at $\lambda$ nm and $a_0$, $a_1$, $a_2$, $a_3$, $a_4$ are constants derived empirically as 0.283, −2.753, 1.457, 0.659 and −1.403, respectively.

The red-NIR band ratio algorithm (RNIR) of the second group has been applied to monitoring Chl-a in inland and coastal waters [13,14,17,18,36,39] and in turbid productive waters using mainly MODIS imagery [34]. A representative algorithm of this group was formulated by Gilerson *et al.* [40] as:

$$C_{Chla} = c_1 \frac{R_{rs}\,(748)}{R_{rs}\,(667)} + c_2 \quad (2)$$

where $c_1$ and $c_2$ are constants determined by the relationship between the MODIS image data and the measured Chl-a concentration data.

### *3.2. New Algorithm Development*

The OC3M and RNIR algorithms have been derived empirically and are known to be of low accuracy in coastal waters, such as those present study areas. To improve the accuracy, we have developed a new versatile algorithm that considers the fundamental physics of the relationship between MODIS image data and *in situ* Chl-a concentrations.

First, we recall that reflectance at the wavelength, λ, observed by remote sensing, $R_{rs}(\lambda)$ is the ratio of water-leaving radiance, $L_w(\lambda)$ to down-welling irradiance and $E_d(\lambda)$ just above the sea surface. $R_{rs}(\lambda)$ is directly proportional to the backscattering coefficient, $b(\lambda)$ and inversely proportional to the sum of the absorption $a(\lambda)$ and $b(\lambda)$ as observed in the next equation, which is adapted from Lee *et al.* [41]:

$$R_{rs}(\lambda) = \frac{L_w(\lambda)}{E_d(\lambda)} = \frac{f(\lambda)t^2}{Q(\lambda)n^2} \times \frac{b(\lambda)}{[a(\lambda) + b(\lambda)]} \quad (3)$$

where $f(\lambda)$ is an empirical factor averaging about 0.32–0.33 [21,42–44], $Q(\lambda)$ is the upwelling irradiance-to-radiance ratio $E_u(\lambda)/L_u(\lambda)$, $t$ is the transmittance of the air-sea interface and $n$ is the real part of the index of refraction of seawater.

As an application to the MODIS wavebands in blue to green spectra, the $f(\lambda)t^2/Q(\lambda)n^2$ is appropriately assumed to be constants (*const*) based on the relationship between the $f(\lambda)t^2/Q(\lambda)n^2$ and the backscattering by the sea-viewing wide field-of-view sensor (SeaWiFS) at the wavelengths 443, 490 and 555 nm by Barnard *et al.* [45] and the Chl-a algorithm for coastal waters by Carder *et al.* [46]. Additionally, many studies have confirmed that $b(\lambda)$ is usually much smaller than $a(\lambda)$ and can thus be safely removed from the denominator of Equation (3) [21], except for highly turbid waters. In the case of phytoplankton-dominated waters, like Tien Yen Bay, Equation (3) can be greatly simplified to:

$$R_{rs}(\lambda) \cong const \times \frac{b(\lambda)}{[a(\lambda) + b(\lambda)]} \approx const \times \frac{b(\lambda)}{a(\lambda)} \quad (4)$$

The total backscattering coefficient, $b(\lambda)$ can be calculated as the sum of two components originating from pure seawater, $b_w(\lambda)$, and particles, $b_p(\lambda)$, as:

$$b(\lambda) = b_w(\lambda) + b_p(\lambda) \quad (5)$$

where $b_w(\lambda)$ is constant [47] and too small in comparison to $b_p(\lambda)$ [48,49]; thus $b(\lambda)$ is equal nearly to $b_p(\lambda)$. Therefore, Equation (4) can be transformed into:

$$R_{rs}(\lambda) = const \times \frac{b(\lambda)}{a(\lambda)} \cong const \times \frac{b_p(\lambda)}{a(\lambda)} \quad (6)$$

The term "*const*" in Equation (6), then, is eliminated in the ratio of two reflectances at visible blue, 443 nm, and visible green, 551 nm. This ratio, $R$, can be expressed simply by the absorption factor when $b(443)/b(551)$ is assumed to be 1.

$$R = \frac{R_{rs}(443)}{R_{rs}(551)} = \frac{b_p(443).a(551)}{a(443).b_p(551)} = \frac{a(551)}{a(443)} \quad (7)$$

The appropriateness of the assumption that $b(443)/b(551)$ is equal to 1 was proven through the measurement results of inherent optical properties of phytoplankton-rich coastal waters [37,50,51]. In addition, the values of $b(443)$ and $b(551)$ are almost the same in the coastal waters containing Chl-a > 2 mg/m$^3$ [52,53], which is supported by the observation of Schalles [4], that the effect of particle backscattering on reflectances from blue to green wavelengths can be negligible for waters containing Chl-a > 2 mg/m$^3$. *In situ* data in Tien Yen Bay in July 2010, showed that the Chl-a concentrations ranged from 8.1 to 16.5 mg/m$^3$. Therefore, the above assumptions can be applied to the waters of Tien Yen Bay.

In the case of water with an unknown range of *in situ* Chl-a concentration, $b(443)/b(551)$ is not assumable as 1. Then, *in situ* spectroradiometric measurement is necessary to determine the water surface reflectance and inherent optical properties, such as the $a(\lambda)$ and $b(\lambda)$ coefficients. After this determination, Chl-a concentration can be calculated directly using the backscattering algorithms [37,54].

For general ocean water, $a(\lambda)$ can be spectrally divided into four absorption components originating from pure water ($a_w$), phytoplankton ($a_p$), detritus or non-algal particles ($a_{NAP}$), and gelbstoff or colored dissolved organic matter ($a_{CDOM}$) [34] as:

$$a(\lambda) = a_w(\lambda) + a_p(\lambda) + a_{NAP}(\lambda) + a_{CDOM}(\lambda) \quad (8)$$

Based on the measurement results of $a_p(\lambda)$, $a_{NAP}(\lambda)$ and $a_{CDOM}(\lambda)$ at the 350 stations in various coastal waters around Europe, it was concluded that the $a_{NAP}(\lambda)$ and $a_{CDOM}(\lambda)$ were negligibly small, and the $a_w(\lambda)$ was constant regardless of $\lambda$ [55]. Accordingly, Equation (8) can be simplified as $a(\lambda) \cong a_p(\lambda) + const$, and Equation (7) is transformed into:

$$R = \frac{a(551)}{a(443)} = \frac{a_p(551) + const.}{a_p(443) + const.} \quad (9)$$

In this equation, Chl-a concentration is a function of $a_p(\lambda)$ only:

$$a_p(\lambda) = a_p^*(\lambda) \cdot C_{Chl-a} \quad (10)$$

where $a^*_p(\lambda)$ denotes a chlorophyll-specific absorption coefficient of phytoplankton ($m^2/mg$) at a unit concentration of Chl-a (1 $mg/m^3$), as shown in Figure 2. Equation (8) can be rewritten as:

$$R = \frac{a(551)}{a(443)} = \frac{a_p^*(551) \cdot C_{Chl-a} + \alpha}{a_p^*(443) \cdot C_{Chl-a} + \beta} \quad (11)$$

$$C_{Chl-a}\left(R \cdot a_p^*(443) - a_p^*(551)\right) = \alpha - R \cdot \beta \quad (12)$$

where $\alpha$, $\beta$ are constants.

As $a^*_p(551)$ is negligible, *i.e.*, $a^*_p(443) >> a^*_p(551)$ ([4]; Figure 2), the following approximation holds:

$$R \cdot a_p^*(443) - a_p^*(551) \cong R \cdot a_p^*(443) \quad (13)$$

Consequently, Chl-a concentration can be estimated by:

$$C_{Chla} = \frac{\alpha - R \cdot \beta}{R \cdot a_p^*(443)} = \omega \cdot R^{-1} + \varepsilon = \omega \frac{R_{rs}(551)}{R_{rs}(443)} + \varepsilon \quad (14)$$

where $\omega$ and $\varepsilon$ are constants inversely proportional to $a^*_p(443)$ and determined by the relationship between the MODIS data and *in situ* Chl-a data. This algorithm, using the reflectance ratio of the green and blue bands, is termed "rGBr" hereafter. The performance of rGBr is evaluated for Tien Yen Bay by comparing the two existing algorithms, OC3M and RNIR, as described below.

From the absorption spectra of the phytoplankton classes in different sizes, the use of blue and green bands (443 and 511 nm, respectively) has been demonstrated to be valid for Chl-a concentration in tropical or low latitude waters, because micro-phytoplankton is mostly accumulated in the surface layer [54–56]. This condition is applicable to Tien Yen Bay.

Furthermore, bottom reflectance tends to affect $R_{rs}(\lambda)$ significantly in usual coastal shallow waters [57,58]. A $R_{rs}(410)/R_{rs}(670)$ algorithm then was proposed to estimate Chl-a concentration instead of the traditional blue-to-green band-ratio algorithm [57]. This new algorithm was proven to be

accurate only for the waters with low Chl-a concentration <1 mg/m$^3$ [58]: its availability for the eutrophic waters with Chl-a > 10 mg/m$^3$ has been uncertain. Therefore, *in situ* measurement of turbidity or water transparency is necessary to monitor Chl-a concentration in shallow waters using rGBr.

### *3.3. Geostatistical Methods*

Pixel-based satellite images of the Earth's surface are often composed of spatially and temporally irregular datasets due to missing swaths or cloud coverage. Additionally, due to limitations in spatial resolution, maps produced directly from satellite image data may lack the detail and accuracy required for environmental monitoring. To compensate for missing image data and to improve the spatial resolution of MODIS image data, geostatistics has been adopted. The effectiveness of geostatistics has been demonstrated by many case studies for improving the spatial resolution of satellite imagery [59–63] and mapping distributions of Chl-a and total suspended solids concentrations [33,64–68]. Therefore, geostatistics must be the most promising for the present purpose.

Geostatistics uses the semivariogram, $\gamma(h)$, to quantify the spatial correlation of a regionalized variable by the mean variability between two points:

$$\gamma(h) = \frac{1}{2N(h)} \sum_{i=1}^{N(h)} \{Z(x_i) - Z(x_i + h)\} \quad (15)$$

where $Z(x_i)$ is the estimated Chl-a concentration at pixel $i$, $h$ is the lag distance between two pixels of the image and $N(h)$ is the number of pixel pairs of $(x, x + h)$ separated by $h$. The experimental $\gamma(h)$ in Equation (15) is then approximated by a model, such as the spherical model, and the parameters that describe the structure of spatial variation, range, sill and the nugget effect are determined.

Spatial interpolation using $\gamma(h)$ is termed kriging. Of the various methods, ordinary kriging (OK), as shown in the next equation, is the most widely used univariate, non-biased method:

$$\begin{cases} Z^*(x_p) = \sum_{i=1}^{n} \lambda_i Z(x_i) \\ \sum_{j=1}^{n} \lambda_j = 1 \end{cases} \quad (16)$$

where $Z^*(x_p)$ is a satisfactory estimate of OK, $\lambda_i$ is the weight of $Z(x_i)$ and $n$ is the number of data used for the interpolation. $\lambda_I$ can be obtained by solving the linear equation related to $\gamma(h)$.

## 4. Results and Discussion

### *4.1. Atmospheric Correction*

The atmospheric correction methods, DOS and QUAC, were applied to the MODIS 36 band data to obtain $R_{rs}(\lambda)$ at the locations involving the sampling points. Table 1 summarizes the descriptive statistics of $R_{rs}(\lambda)$ at the five primary ocean color bands (Bands 9, 10, 12, 13 and 15). Almost all electromagnetic reflectances are absorbed by water in the wavelength of visible red, near infrared and short-wave infrared regions. The QUAC-corrected spectra in these regions are known to become similar spuriously to water body spectra [63]. In fact, the $R_{rs}(\lambda)$ data was not obtained for Bands 12, 13

and 15, corresponding to part of the visible red and near-infrared regions by QUAC, as shown by the mark "not a number (NaN)". Therefore, QUAC is not applicable to the MODIS image data of tropical coastal waters. The suitability of DOS to Tien Yen Bay is proven by this study in addition to Ha and Koike [33]. The DOS gives an effective cross-calibration for Bands 9, 10 and 12 particularly, because there are no pixels that cannot be corrected in the sampled 40 pixels (Table 1).

**Table 1.** Descriptive statistics of reflectance data obtained at 40 pixels of the Moderate Resolution Imaging Spectroradiometer (MODIS) image data corresponding to the locations of water sampling points. Two atmospheric correction methods, dark-object subtraction (DOS) and Quick Atmospheric Correction (QUAC), were used to determine the reflectance at primary ocean color bands. NaN stands for "not a number".

| | **Data Obtained from DOS for Bands** | | | | | **Data Obtained from QUAC for Bands** | | | | |
|---|---|---|---|---|---|---|---|---|---|---|
| | 9 | 10 | 12 | 13 | 15 | 9 | 10 | 12 | 13 | 15 |
| Average | 0.043 | 0.040 | 0.042 | 0.022 | 0.036 | 0.117 | 0.039 | NaN | NaN | NaN |
| Maximum | 0.077 | 0.082 | 0.090 | 0.036 | 0.010 | 0.147 | 0.072 | NaN | NaN | NaN |
| Minimum | 0.026 | 0.021 | 0.015 | 0.010 | 0.024 | 0.065 | 0.039 | NaN | NaN | NaN |
| Out of 40 pixels | 0 | 0 | 0 | 13 | 8 | 0 | 0 | 40 | 40 | 40 |

### *4.2. Estimation Algorithm for Chl-a Concentrations*

The 443 and 551 nm wavelengths used for estimating Chl-a concentration are equivalent to MODIS Bands 9 and 12, respectively. Using $R_{rs}(443)$ and $R_{rs}(551)$ obtained through DOS and the least squares method for the relationship between their ratio ($R$ in Equation (7)) and the Chl-a concentrations at the 40 points (Figure 2a), the rGBr of Equation (14) was determined as:

$$C_{Chla} = 8.843 \cdot R + 4.093 \quad (17)$$

The descriptive statistics of the Chl-a concentrations estimated at 392 pixels by rGBr are shown in Table 2, which are similar to those of the sample data. In addition, the estimated values are well fitted to the measured values with a correlation coefficient $r = 0.78$, as confirmed in Figure 2b. The relative error of this estimation ranges from zero to 15%, and the root mean square error (RMSE) is small at 1.13 mg/m$^3$ (Table 3) against the data average of 12.5 mg/m$^3$ (Table 2).

Table 3 compares the prediction accuracy of rGBr with that of OC3M of Equation (1) and RNIR of Equation (2). These equations were also determined by $R_{rs}$ and the measured concentration data using the least squares method. It is evident that rGBr has the largest $r$ and the smallest mean standard error (MSE) and RMSE.

The capabilities of the three models can be evaluated, as seen in Figure 3, which shows the relationship between the measured and estimated Chl-a concentrations. As estimated from the $r$ value, this relationship is the weakest in RNIR: in particular, the high and low concentrations cannot be estimated. This result proves the overestimation problem of RNIR for the waters containing Chl-a ≥ 6 mg/m$^3$ by Gilerson *et al.* [40]. The difference between OC3M and rGBr is remarkable in the region with concentrations higher than 14 mg/m$^3$, in which the trend of the underestimate is stronger in OC3M than rGBr. Consequently, rGBr was identified as the best model for estimating Chl-a concentrations over Tien Yen Bay with small errors.

**Figure 2.** (**a**) The relationship between chlorophyll-a (Chl-a) concentration of the water sample and the ratio of two reflectances at MODIS Band 12 (551 nm) *vs.* Band 9 (443 nm). A regression line is drawn to show the relationship. (**b**) Scattergram of Chl-a concentrations between the sample value and estimation by the ratio of green and blue band reflectance (rGBr) of Equation (17). The 45-degree dotted line denotes perfect estimation.

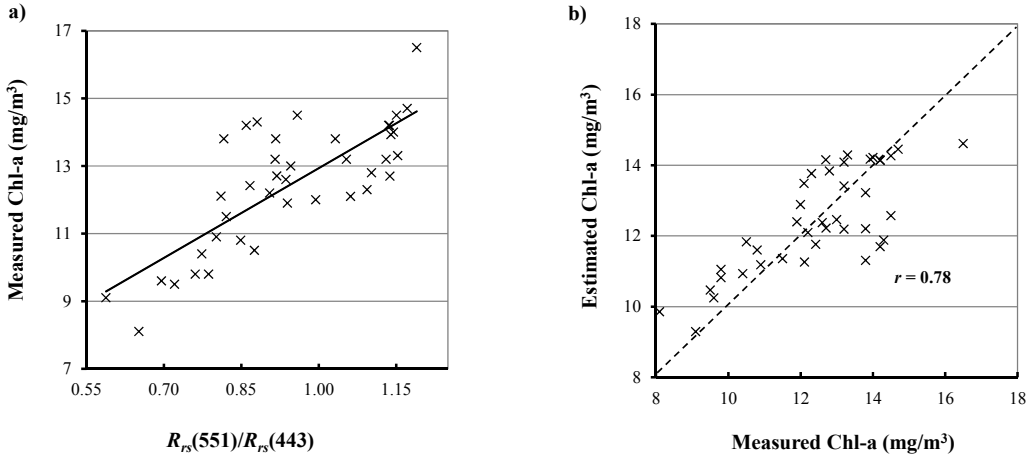


**Table 2.** Descriptive statistics of three datasets of Chl-a concentrations (mg/m$^3$): water samples, estimations from the MODIS image data by rGBr and predictions at the MODIS pixels by cross-validation of ordinary kriging (OK).

| | Sample Data | Estimation from MODIS | Prediction by OK |
|---|---|---|---|
| Number of data | 40 | 392 | 392 |
| Mean | 12.5 | 13.3 | 13.3 |
| Median | 12.7 | 13.3 | 13.3 |
| Maximum | 16.5 | 16.6 | 16.1 |
| Minimum | 8.1 | 9.0 | 9.9 |
| Standard deviation | 1.8 | 1.4 | 1.3 |
| Range | 8.4 | 7.6 | 6.3 |

**Table 3.** Comparison of three algorithms for estimating the accuracy of Chl-a concentrations. The accuracy is evaluated by the linear correlation coefficient (*r*), mean square error (MSE) and root mean square error (RMSE) for the 40 sample values. RNIR, red-near-infrared band ratio algorithm (RNIR).

| Algorithm | Models with Empirical Coefficients | *r* | MSE (mg/m$^3$) | | | RMSE (mg/m$^3$) |
|---|---|---|---|---|---|---|
| | | | Average | Max | Min | |
| OC3M (O'Reilly *et al.*, 2000) | $C_{Chla} = 10^{1.10-0.42\phi+7.09\phi^2-130.13\phi^3-421.26\phi^4}$ where $\phi = \log 10\{\frac{\max[R_{rs}(443):R_{rs}(488)]}{R_{rs}(551)}\}$ | 0.65 | 1.19 | 5.48 | 0.03 | 1.70 |
| RNIR (Gilerson *et al.*, 2010) | $C_{Chla} = -51.212\frac{R_{rs}(748)}{R_{rs}(667)} + 63.084$ | 0.43 | 1.48 | 4.19 | 0.23 | 1.82 |
| rGBr | $C_{Chla} = 8.843\frac{R_{rs}(551)}{R_{rs}(443)} + 4.093$ | 0.78 | 0.90 | 2.51 | 0.05 | 1.13 |

**Figure 3.** Scattergram of Chl-a concentrations between the sample value and estimation by three algorithms. The 45-degree dotted line denotes perfect estimation.

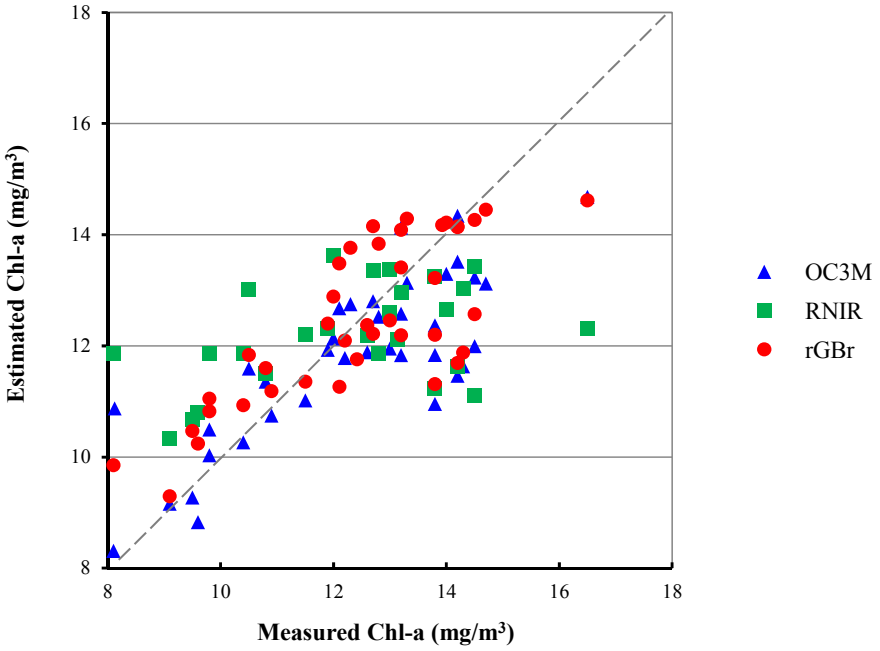


*4.3. Spatial Distribution of Chl-a Concentrations*

The spatial distribution of Chl-a concentrations within Tien Yen Bay was estimated by applying rGBr to the MODIS image data, as illustrated in Figure 4. Although a rough trend of the distribution is apparent in this 1 km interval estimation of the 392 pixels (e.g., the locations of the highest and lowest values), there is no precise variation near the shoreline. Additionally, estimation is inevitably impossible for areas covered by clouds, as shown in black in Figure 4. It can be confirmed therefore that using only MODIS image data is not effective for monitoring the spatial-temporal changes of Chl-a concentrations that may have large variation in bad weather conditions.

Next, the MODIS-based estimation was transformed by OK into a more precise distribution with a 100-m grid. Usually, *in situ* sample data are used for OK, but Chl-a concentrations cannot be estimated on the day without sample data by this usual procedure. Instead, estimates of Chl-a concentrations using only MODIS image data enable Chl-a monitoring on the image acquisition day. The histogram of the 392 Chl-a concentration data is not far from a normal distribution (Figure 5). Therefore, this dataset is suitable for geostatistical analyses that require normal distribution of regionalized random variables as OK.

Experimental $\gamma(h)$ produced from the dataset was approximated best by the exponential model with a nugget effect of zero, a sill of 1.6 mg/m$^3$ and a range of 17.9 km (Figure 6a). To check the spatial estimation accuracy of OK with a cross-validation, a scattergram that represents the relationship between the original $C_{Chla}$-value at a particular MODIS pixel (estimations in Table 1) and the predicted OK value using the $C_{Chla}$ data around the target pixel (predictions in Table 2) was produced (Figure 6b). The resultant mean error of the prediction is close to zero (0.017 mg/m$^3$), and the RMSE is relatively low (0.43 mg/m$^3$), which confirms the high capability of OK. The resultant OK distribution

of Chl-a concentration and the kriging variance map are depicted in Figure 7. The kriging variances are negligible over the entire bay. Only the zone covered by clouds has a relatively high variance, but its value is smaller than 3% of the estimated $C_{Chla}$. Such a variance trend also supports the correctness of the OK estimation.

**Figure 4.** Spatial distribution of Chl-a concentrations over Tien Yen Bay on 6 July 2010, with a 1-km interval using MODIS image data and rGBr.

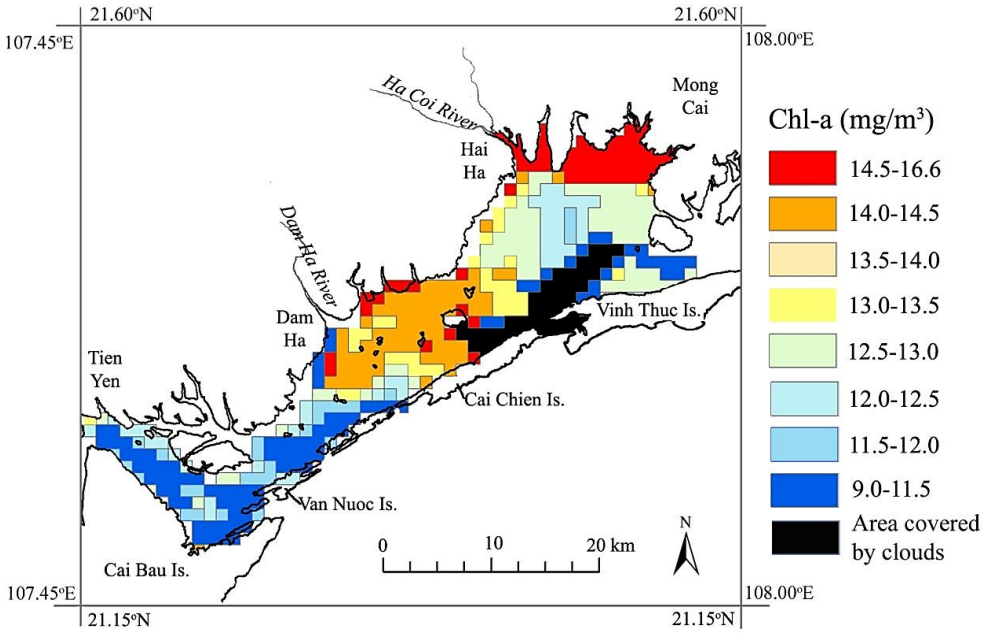


**Figure 5.** Histogram of Chl-a concentrations estimated from MODIS/Terra image data and rGBr.

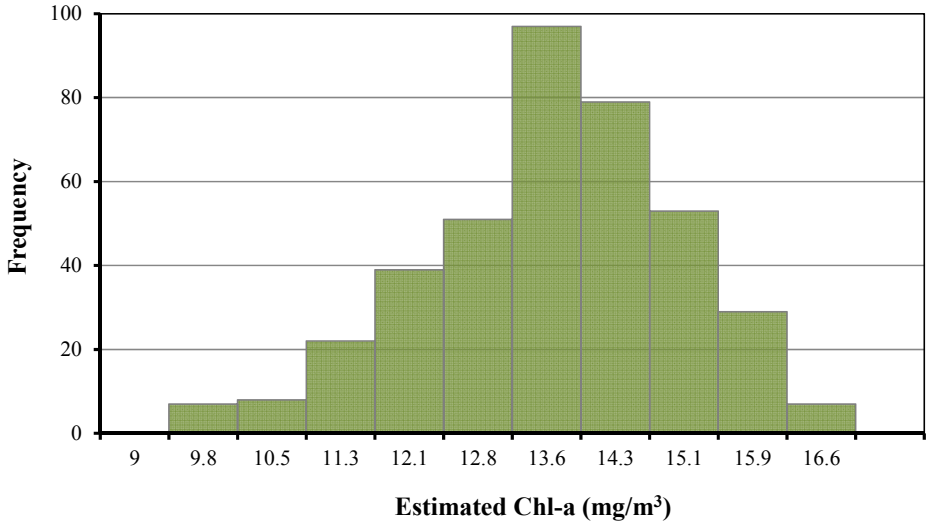


The OK map in Figure 7 presents much more precise spatial characteristics than the original $C_{Chla}$ distribution in Figure 4 and also clarifies the eutrophic conditions in the waters of Tien Yen Bay. The Chl-a concentrations on 6 July 2010, ranged from nine to 16.6 mg/m$^3$, which are four to 7.5 times of

the eutrophic level, 2.21 mg/m$^3$ [71:Table 4]. Generally, concentrations of Chl-a over 14.5 mg/m$^3$ occur in local estuaries at the mouths of the Ha Coi and Dam Ha Rivers and along the coast from Mong Cai to Hai Ha. The middle bay also contains high Chl-a from 13.5 to 14.5 mg/m$^3$ from Cai Chien to Hai Ha districts. On the contrary, the concentrations become low toward the west near Cai Bau Island, with a minimum of 9 mg/m$^3$ in the channels connected with the outer sea.

**Figure 6.** (**a**) Omnidirectional experimental semivariogram and exponential model (curve) of the Chl-a concentrations estimated from MODIS data and rGBr. (**b**) Scattergram for cross-validation of ordinary kriging prediction. The 45-degree dotted line is superimposed.

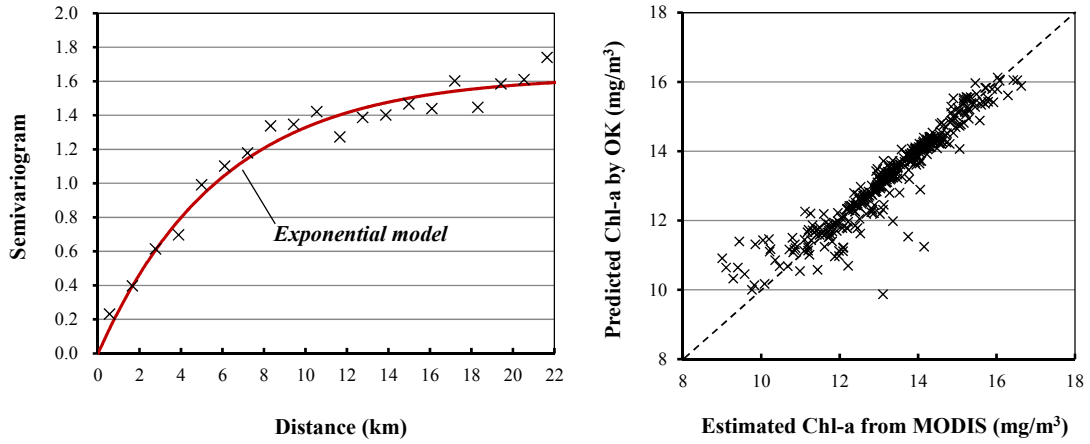


**Figure 7.** (**a**) Spatial distribution of Chl-a concentrations produced by interpolating the MODIS image-based estimation in Figure 4 using OK and a 100-m grid size. (**b**) Kriging variance for representing the uncertainty of estimation of Chl-a concentrations by OK. in the image, no space before and after en dash representing ranges.

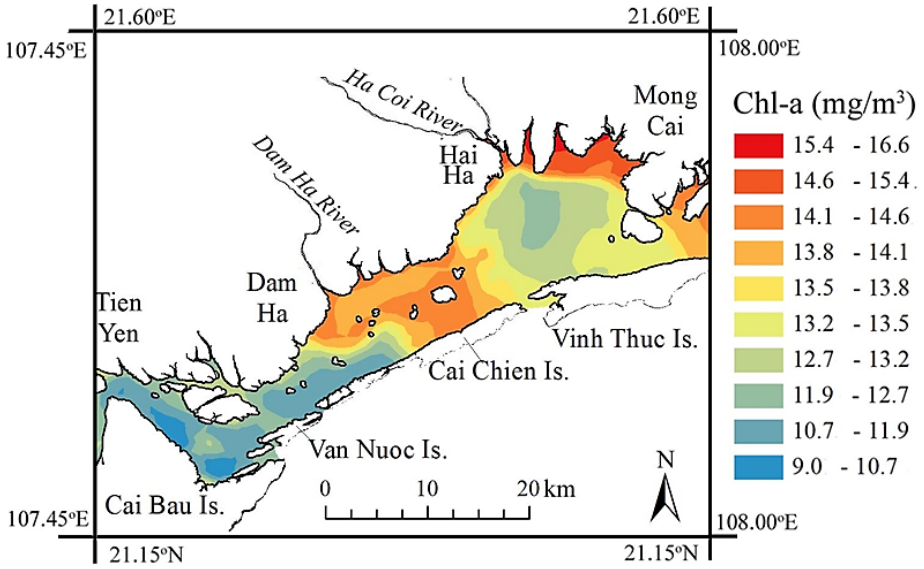

**Figure 7.** *Cont.*

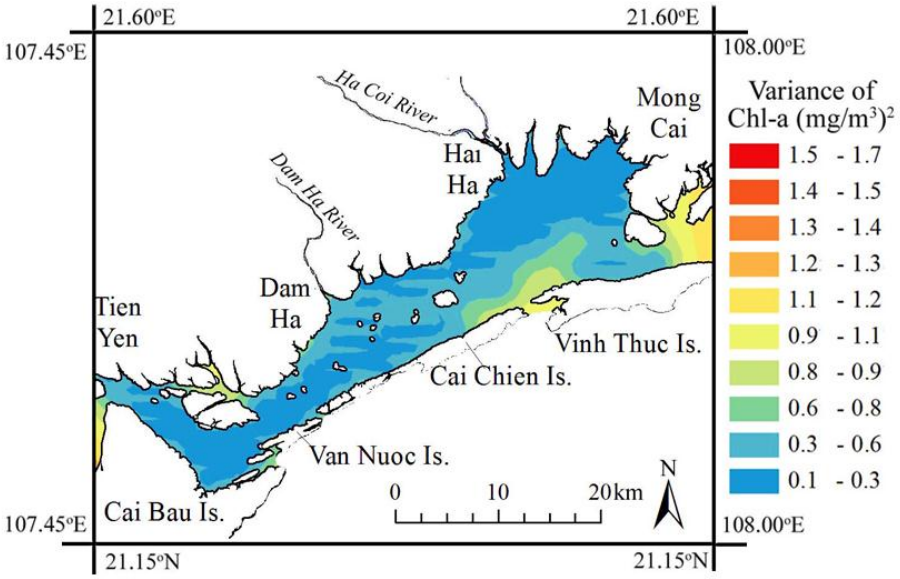


(**b**)

Those spatial characteristics conform to the hydrodynamic system in the bay that is generated by the interaction of regional surface currents ([72]; Figure 4), tides and waves. The local river estuaries and central bay are shielded by the islands (Van Nuoc, Cai Chien and Vinh Thuc) and the tortuous coastline, and therefore, the hydro-energy related to currents and waves is weak there. Under such conditions, phytoplankton, the main source of high Chl-a concentrations, accumulate and grow. In contrast, in the connection channels and the largely movable waters affected directly by the outer sea, the hydro-energy is strong. These waters contain high amounts of re-suspended material, which prevent the accumulation and growth of phytoplankton. Accordingly, Chl-a concentrations become low in such high-energy zones.

### *4.4. Eutrophication Processes over the Course of a Year*

To clarify the eutrophication process and the seasonal change of Chl-a concentrations in the waters of Tien Yen Bay, the rGBr and OK were applied to 21 scenes of MODIS image data that were acquired under the lowest cloud coverage conditions from late May 2010, to middle May 2011. The resultant maps are shown in Figure 8. The general trend of the Chl-a concentrations is observed to be similar to Figure 7 in that higher concentrations are located in the near shore and the central bay waters, while lower concentrations are distributed in the waters connected directly to the outer sea. The map of 5 August 2010, reveals extraordinarily high concentrations over the whole bay, which may have been caused by the massive growth of phytoplankton, due to the strong solar energy in the midsummer.

The seasonal trend is highlighted by the graphs in Figure 9 showing monthly averaged, maximum and minimum Chl-a concentrations over Tien Yen Bay calculated from the maps in Figure 8. The Chl-a concentrations (monthly averaged concentrations) reached a maximum of 16.6 mg/m$^3$ in August 2010. After that, the concentrations declined toward the winter, with a minimum of 12.0 mg/m$^3$ in January 2011, and then increased again toward a second maximum concentration (15.9 mg/m$^3$) in March 2011.

**Figure 8.** Spatio-temporal changes of Chl-a concentrations for the year from May 2010, to May 2011, over Tien Yen Bay produced from 21 MODIS scene data, rGBr and OK.

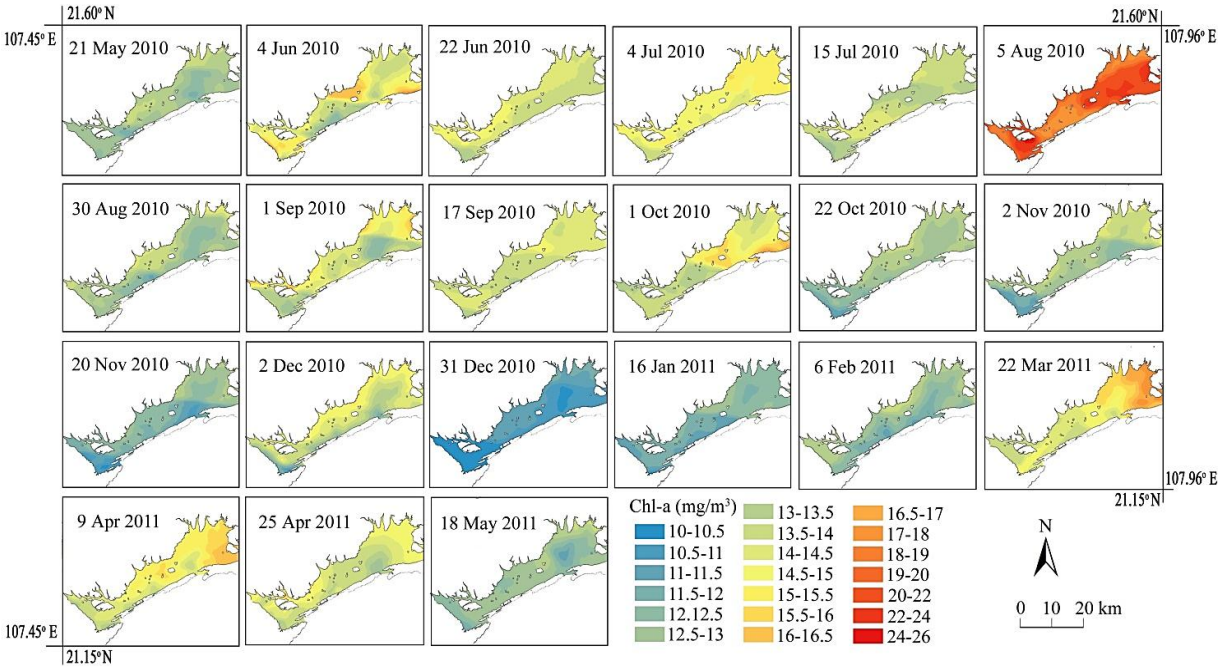


The monthly maximum and minimum draw similar trends to the average. These temporal changes are coincident with the monthly averaged air temperature and monthly precipitation [73]. Because solar energy input in the early spring is not great enough for the rapid growth of phytoplankton, the concentrations decline to a general level soon after the second peak. In many coastal waters, such as the southern coast of Hokkaido in northern Japan [74], Chl-a concentrations usually show a bimodal variation with the first peak in spring and the second peak in late summer to early autumn. This trend coincides with that observed in the waters of Tien Yen Bay.

CSTT [75] defined 10 mg/m$^3$ of Chl-a as the Environmental Quality Standard for coastal waters. If the Chl-a concentration of a water body frequently exceeds this criterion in the summer, it is regarded as having a eutrophic condition. Based on this criterion, the waters of Tien Yen Bay were considered to be eutrophic over the entire study period, with the degree of eutrophication being the strongest midsummer. However, undesirable eutrophication disturbances, such as algae blooms, generated in the water with Chl-a over 100 mg/m$^3$ [76] have not been observed in Tien Yen Bay. This bay may be eutrophic by natural processes rather than by anthropogenic causes, such as wastewater, thereby maintaining a high ecological quality similar to other coastal areas [24]. The natural cause is suggested by the positive moderate correlation of the Chl-a concentrations with the meteorological factors as shown in Figure 9 ($r$ = 0.57 and 0.54 for the air temperature and precipitation, respectively) and no specific accumulation of Chl-a concentrations in a certain area.

Note that the remote sensing technique can detect Chl-a in surface waters only. However, Tien Yen Bay is a shallow water body; then, Chl-a concentrations may be relatively uniform over the depth except for the deep channels [28]. Phytoplankton, such as diatoms (Bacillariophyta), is often accumulated at the highest level in the surface water layer within the 1-m depth for photosynthesis.

**Figure 9.** Variations of monthly averaged, maximum and minimum Chl-a concentrations over Tien Yen Bay calculated from the maps in Figure 8 and their correlations with monthly averaged air temperature (**a**) and monthly precipitation (**b**). The *r* values denote the correlations of the monthly averaged Chl-a concentration with those meteorological factors.

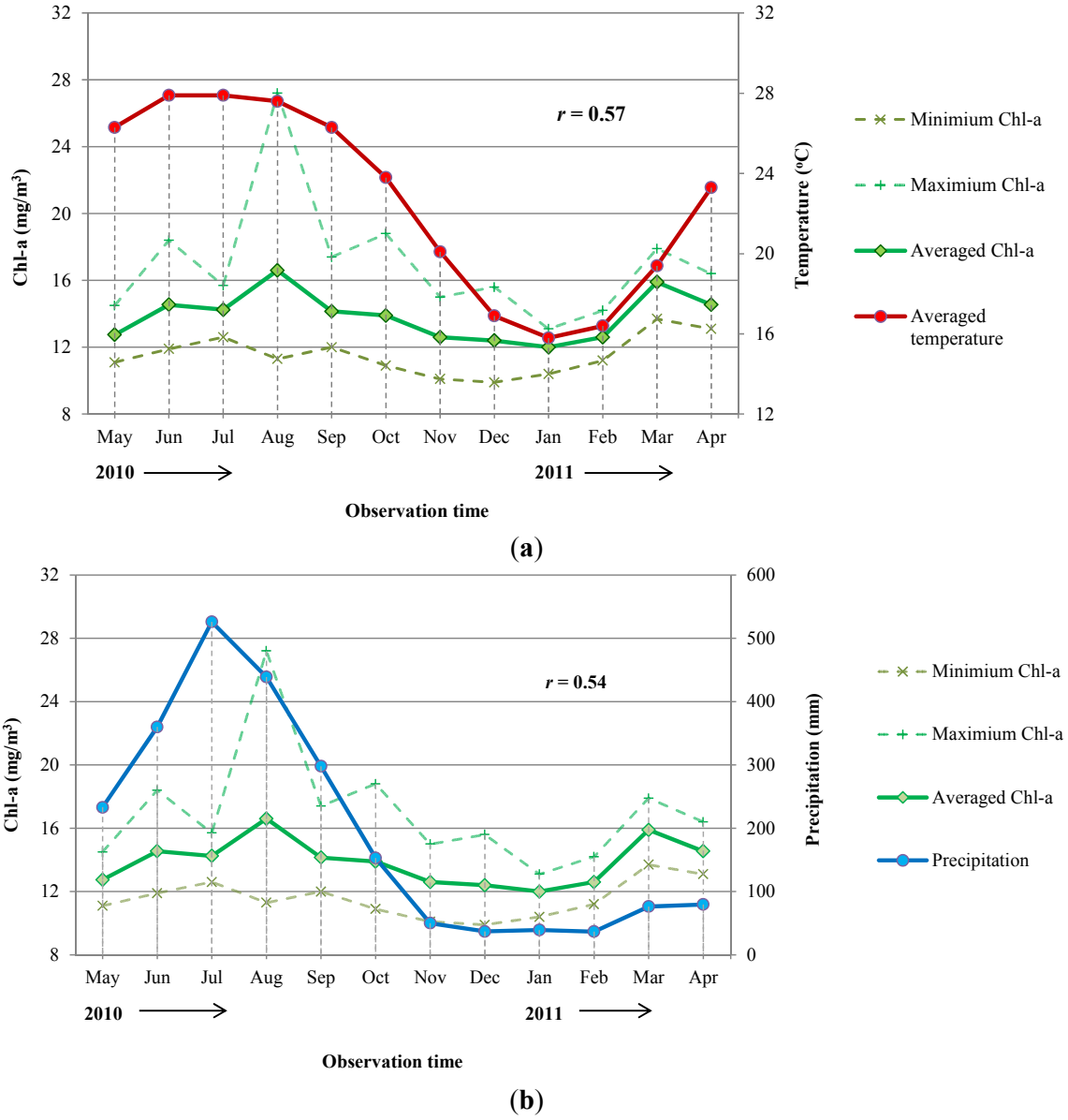


## 5. Conclusions

To improve the accuracy of Chl-a concentration estimates in phytoplankton-rich coastal waters using MODIS image data, the most representative sea-observation satellite imagery, we developed an algorithm that considers the bio-optical properties of coastal waters and adopted geostatistics as a post-processing technique for down-scaling spatial resolution. The main results obtained are summarized as follows:

(1) Two widely-used atmospheric correction methods, DOS and QUAC, were compared to obtain reflectance at the sea surface by excluding atmospheric contributions from the MODIS image data. DOS was identified to be more suitable for tropical waters, such as those of Tien Yen Bay.

(2) Consideration of the optical properties of water shows that the concentration of Chl-a can be physically calculated by the ratio of the reflectances of the seawater surface at the visible green and blue wavelengths. The Chl-a concentrations in phytoplankton-rich coastal waters estimated by the proposed algorithm, rGBr, fit the measured *in situ* concentrations better and with smaller errors than the two previous representative algorithms, OC3M and RNIR.

(3) The effectiveness of OK to improve the spatial resolution of the MODIS image-based estimation of Chl-a concentration from 1 km to 100 m was demonstrated. This improvement was possible because the OK map clarified the variation of Chl-a concentration in detail, particularly in local estuaries. From that OK map, the hydrodynamic system in Tien Yen Bay is suggested to be a main factor controlling the distribution of Chl-a concentrations.

(4) By applying the rGBr and OK to the 21 scenes of MODIS image data from May 2010 to May 2011, notable features and seasonal trends were detected. In particular, the Chl-a concentrations have a bimodal variation. Furthermore, the waters of Tien Yen Bay can be labeled as naturally eutrophic, because of Chl-a values higher than 10 $mg/m^3$ in the summer. This natural cause is supported by the correlation of Chl-a concentrations with representative meteorological factors, air temperature and precipitation.

In conclusion, the combination of the proposed rGBr and OK methods can contribute to monitoring water quality and the eutrophication process in tropical coastal areas having similar geomorphological conditions as Tien Yen Bay, particularly in the South China Sea coast, where this is recognized as the global marine center of shallow-water tropical biodiversity.

## Acknowledgments

We are grateful to the projects coded QGTD 10.31 TRIG-A and 105.09.82.09 NAFOSTED by the Vietnamese National Scientific Grant for their support of the fieldwork and water sample analysis. Thanks also go to NASA for providing the MODIS data and to four anonymous reviewers for their valuable comments and suggestions that helped improve the clarity of the manuscript.

## Conflicts of Interest

The authors declare no conflict of interest.

## References

1. Matthews, A.M.; Duncan, A.G.; Davison, R.G. An assessment of validation techniques for estimating chlorophyll-a concentration from airborne multispectral imagery. *Int. J. Remote Sens.* **2001**, *22*, 429–447.
2. Cauwer, V.D.; Ruddick, K.; Park, Y.J.; Nechad, B.; Kyramarios, M. Optical remote sensing in support of eutrophication monitoring in the southern North Sea. *EARSeL eProc.* **2004**, *3*, 208–221.

3. Zimba, P.V.; Gitelson, A. Remote estimation of chlorophyll concentration in hyper-eutrophic aquatic systems: Model tuning and accuracy optimization. *Aquaculture* **2006**, *256*, 272–286.
4. Schalles, J.F. Optical Remote Sensing Techniques to Estimate Phytoplankton Chlorophyll-a Concentrations in Coastal Waters with Varying Suspended Matter and CDOM Concentrations. In *Remote Sensing of Aquatic Coastal Ecosystem Processes: Science and Management Application*; Richardson, L.L., LeDew, E.F., Eds.; Springer: Dordrecht, The Netherlands, 2006; pp. 27–78.
5. Ibrahim, A.N; Mabuchi, Y.; Murakami, M. Remote sensing algorithms for monitoring eutrophication in Ishizuchi storm water reservoir in Kochi Prefecture, Japan. *Hydrol. Sci. J.* **2009**, *50*, 525–542.
6. Gordon, H.R; Morel, A.Y. *Remote Assessment of Ocean Color for Interpretation of Satellite Visible Imagery: A Review*; Springer-Verlag: New York, NY, USA, 1983; pp. 1–114.
7. Aiken, J.; Moore, G.F.; Trees, C.C.; Hooker, S.B.; Clark, D.K. The SeaWiFS CZCS-Type Pigment Algorithm. In *SeaWiFS Technical Report Series*; Hooker, S.B., Firestone, E.R., Eds., NASA Goddard Space Flight Center: Greenbelt, MD, USA, 1995; Volume 29, pp. 1–34.
8. O'Reilly, J.E.; Maritorena, S.; Mitchell, B.G.; Siegel, D.A.; Carder, K.L.; Garver, S.A.; Kahru, M.; McClain, C. Ocean color chlorophyll algorithms for SeaWiFS. *J. Geophys. Res.* **1998**, *103*, 24937–24953.
9. O'Reilly, J.E.; Maritorena, S.; Mitchell, B.G.; Siegel, D.A.; Carder, K.L.; Garver, S.A.; Kahru, M.; McClain, C. Ocean Color Chlorophyll a Algorithms for SeaWiFS, OC2, and OC4: Version 4. In *SeaWiFS Postlaunch Technical Report Series, Volume 11, SeaWiFS Postlaunch Calibration and Validation Analyses, Part 3*; Hooker, S.B., Firestone, E.R., Eds.; NASA Goddard Space Flight Center: Greenbelt, MD, USA, 2000; pp. 9–23.
10. Carder, K.L.; Steward, R.G.; Harvey, G.R.; Ortner, P.B. Marine humic and fulvic acids: Their effects on remote sensing of ocean chlorophyll. *Limnol. Oceanogr.* **1989**, *34*, 68–81.
11. Gallegos, C.L.; Correll, D.L.; Pierce, J.W. Modeling spectral diffuse attenuation, absorption, and scattering coefficients in a turbid estuary. *Limnol. Oceanogr.* **1990**, *35*, 1486–1502.
12. Ritchie, J.C.; Schiebe, F.R.; Cooper, C.M.; Harrington, J.A., Jr. Chlorophyll measurements in the presence of suspended sediment using broad band spectral sensors aboard satellites. *J. Freshwater Ecol.* **1994**, *9*, 197–206.
13. Schalles, J.F.; Sheil, A.T.; Tycast, J.F.; Alberts, J.J.; Yacobi, Y.Z. Detection of Chlorophyll, Seston, and Dissolved Organic Matter in the Estuarine Mixing Zone of Georgia Coastal Plain Rivers. In Proceedings of the Fifth International Conference on Remote Sensing for Marine and Coastal Environments, San Diego, CA, USA, 5–7 October 1998; pp. 315–324.
14. Gons, H.J. Optical tele-detection of chlorophyll a in turbid inland waters. *Environ. Sci. Technol.* **1999**, *33*, 1127–1132.
15. Hladik, C.M. Close Range, Hyperspectral Remote Sensing of Southeastern Estuaries and an Evaluation of Phytoplankton Chlorophyll-a Predictive Algorithms. M.Sc. Thesis, Creighton University, Omaha, NE, USA, 2004.
16. Vertucci, F.A.; Likens, G.E. Spectral reflectance and water quality of Adirondack mountain region lakes. *Limnol. Oceanogr.* **1989**, *34*, 1656–1672.

17. Schalles, J.F.; Gitelson, A.A.; Yacobi, Y.Z.; Kroenke, A.E. Estimation of chlorophyll a from time series measurements of high spectral resolution reflectance in an eutrophic lake. *J. Phycol.* **1998**, *34*, 383–390.
18. Thiemann, S.; Kaufmann, H. Lake water quality monitoring using hyperspectral airborne data—A semiempirical multisensor and multitemporal approach for the Mecklenburg Lake District, Germany. *Remote Sens. Environ.* **2002**, *81*, 228–237.
19. Kallio, K.; Koponen, S.; Pulliainen, J. Feasibility of airborne imaging spectrometry for lake monitoring—A case study of spatial chlorophyll-a distribution in two meso-eutrophic lakes. *Int. J. Remote Sens.* **2003**, *24*, 3771–3790.
20. McGlathery, K.J.; Sundback, K.; Anderson, I.C. Eutrophication in shallow coastal bays and lagoons: the role of plants in coastal filter. *Marine Ecol. Prog. Series* **2007**, *348*, 1–18.
21. Morel, A.; Prieur, L. Analysis of variations in ocean color. *Limnol. Oceanogr.* **1977**, *22*, 709-722.
22. Wu, M.; Zhang, W.; Wang, X.; Luo, D. Application of MODIS satellite data in monitoring water quality parameters of Chaohu Lake in China. *Environ. Monit. Assess.* **2009**, *148*, 255–264.
23. Vietnam Environment Protection Agency (VEPA), World Conservation Union (IUCN), Mekong Wetlands Biodiversity Conservation and Sustainable Use Programme (MWBP). *Overview of Wetland Status in Vietnam following 15 Years of Ramsar Convention Implementation*; VEPA: Hanoi, Vietnam, 2005; pp. 1–80.
24. Hoang, V.T.; Pham, V.H. Biodiversity in Coastal Zones of Tien Yen—Dam Ha, Quang Ninh Province and Conservation. In Proceeding of the 2nd Vietnam National Conference on Biodiversity (in Vietnamese), Hanoi, Vietnam, 17 October 2010; pp. 61–74.
25. Thuoc, C.V. Phytoplankton in the Tien Yen, Bach Dang and Red River mouths. *Marine Resour. Environ.* **1996**, *3*, 242–248.
26. American Public Health Association (APHA). *Standard Methods for the Examination of Water and Wastewater*, 20th ed.; American Public Health Association: Washington, DC, USA, 1998; pp. E1–E15.
27. Department of Environment, Climate Change and Water NSW. *Waterwatch Estuary Field Mannual: A Manual for On-Site Use in the Monitoring of Water Quality and Estuary Health*; Department of Environment, Climate Change and Water NSW: Sydney, Australia, 2010; pp. 2_6–2_7.
28. Vietnam Ministry of Natural Resources and Environment. *Vietnam Topographic Map*; Scale 1/50,000; Department of Survey Map Publishing House: Hanoi, Vietnam, 2004.
29. Chavez, J.P.S., Jr. An improved dark-object subtraction technique for atmospheric scattering correction of multispectral data. *Remote Sens. Environ.* **1988**, *24*, 459–479.
30. Bernstein, L.S.; Adler-Golden, S.M.; Sundberg, R.L.; Levine, R.Y.; Perkins, T.C.; Berk A.; Ratkowski, A.J.; Felde, G.; Hoke, M.L. A New Method for Atmospheric Correction and Aerosol Optical Property Retrieval for VIS-SWIR Multi- and Hyperspectral Imaging Sensors: QUAC (QUick Atmospheric Correction). In Proceedings of IEEE International Geosciences and Remote Sensing Symposium, Seoul, Korea, 25–27 July 2005; pp. 3549–3552.
31. Hadjimitsis, D.G.; Clayton, C.R.I.; Hope, V.S. An assessment of the effectiveness of atmospheric correction algorithms through the remote sensing of some reservoirs. *Int. J. Remote Sens.* **2004**, *25*, 3651–3674.

32. Hadjimitsis, D.G.; Clayton, C.R.I. Field spectroscopy for assisting water quality monitoring and assessment in water treatment reservoirs using atmospheric corrected satellite remotely sensed imagery. *Remote Sens.* **2011**, *3*, 362–377.
33. Ha, N.T.T.; Koike, K. Integrating satellite imagery and geostatistics of point samples for monitoring spatio-temporal changes of total suspended solids in bay waters: application to Tien Yen Bay (Northern Vietnam). *Frontiers Earth Sci.* **2011**, *5*, 305–316.
34. Moses, W.J.; Gitelson, A.A.; Berdnikov, S.; Povazhnyy, V. Estimation of chlorophyll-a concentration in case II waters using MODIS and MERIS data- successes and challenges. *Environ. Res. Lett.* **2009**, *4*, doi:10.1088/1748-9326/4/4/045005.
35. Carder, K.L.; Chen, F.R.; Cannizzaro, J.P.; Campbell, J.W.; Mitchell, B.G. Performance of the MODIS semi-analytical ocean color algorithm for chlorophyll-a. *Adv. Space Res.* **2004**, *33*, 1152–1159.
36. Gitelson, A. The Peak near 700 nm on Radiance Spectra of algae and water - Relationships of its magnitude and position with chlorophyll concentration. *Int. J. Remote Sens.* **1992**, *13*, 3367–3373.
37. Antoite, D.; Andre, J.M.; Morel, A. Oceanic primary production 2: Estimation of global scale from satellite (coastal zone color scanner) chlorophyll. *Glob. Biogeochem. Cy.* **1996**, *10*, 57–69.
38. D'Sa, E.J.; Miller, R.L. Bio-optical properties in waters influenced by the Mississippi River during low flow conditions. *Remote Sens. Environ.* **2002**, *84*, 538–549.
39. Dall'Olmo, G.; Gitelson, A.A.; Rundquist, D.C. Toward a unified approach for remote estimation of chlorophyll-a in both terrestrial vegetation and turbid productive waters. *Geophys. Res. Lett.* **2003**, *30*, 1938–1941.
40. Gilerson, A.A; Gitelson, A.A.; Zhou, J.; Gurlin, D.; Moses, W.; Ioannou, I.; Ahmed, S. Algorithms for remote estimation of chlorophyll-a in coastal and inland waters using red and near infrared bands. *Opt. Express.* **2010**, *18*, 24109–24125.
41. Lee, Z.P.; Carder, K.L.; Hawes, S.H.; Steward, R.G.; Peacock, T.G.; Davis, C.O. A model for interpretation of hyperspectral remote-sensing reflectance. *Appl. Opt.* **1994**, *33*, 5721–5732.
42. Gordon, H.R.; Brown, O.B.; Jacobs, M.M. Computed relationships between the inherent and apparent optical properties of a flat homogeneous ocean. *Appl. Opt.* **1975**, *14*, 417–427.
43. Jerome, J.H.; Bukata, R.P.; Burton, J.E. Utilizing the components of vector irradiance to estimate the scalar irradiance in natural waters. *Appl. Opt*. **1988**, *27*, 4012–4018.
44. Kirk, J.T.O. Volume scattering function, average cosines, and the underwater light field. *Limnol. Oceanogr.* **1991**, *36*, 455–467.
45. Barnard, A.H.; Ronald, J.; Zaneveld, V.; Pegau, S.W. *In situ* determination of the remotely sensed reflectance and the absorption coefficient: Closure and inversion. *Appl. Opt.* **1999**, *38*, 5108–5117.
46. Carder, K.L.; Chen, F.R.; Lee, Z.; Hawes, S.K.; Cannizzaro, J.P. Case 2 Chlorophyll a. In *MODIS Ocean Science Team Algorithm Theoretical Basis Document*; *Version 7*; NASA Goddard Space Flight Center: Greenbelt, MD, USA, 2003; pp. 4–67.
47. Morel, A. Optical Properties of Pure Water and Pure Seawater. In *Optical Aspects of Oceanography*; Jerlov, N.G., Nielson, E.S., Eds.; Academic Press: London, UK, 1974; pp. 1–24.
48. Smith, R.C.; Baker, K.S. Optical properties of the clearest natural waters (200–800 nm). *Appl. Opt.* **1981**, *20*, 177–184.

49. Twardowski, M.S.; Claustre, H.; Freeman, S.A.; Stramski, D.; Huot, Y. Optical backscattering properties of the "clearest" natural waters. *Biogeosciences* **2007**, *4*, 1041–1058.
50. McKee, D.; Cunningham, A.; Slater, J.; Jones, K.J.; Griffiths, C.R. Inherent and apparent optical properties in coastal waters: A study of the Clyde Sea in early summer. *Estuar. Coast. Shelf Sci.* **2002**, *56*, 369–376.
51. McKee, D.; Cunningham, A. Identification and characterisation of two optical water types in the Irish Sea from *in situ* inherent optical properties and seawater constituents. *Estuar. Coast. Shelf Sci.* **2006**, *68*, 305–316.
52. Whitmire, A.L.; Boss, E.; Cowles, T.J.; Pegau, W.S. Spectral variability of the particulate backscattering ratio. *Opt. Expr.* **2007**, *15*, 7019–7031.
53. Park, Y.J; Ruddick K. Model of remote-sensing reflectance including bidirectional effects for case 1 and case 2 waters. *Appl. Opt.* **2005**, *44*, 1236–1249.
54. Babin, M.; Stramski D.; Ferrari, G.M.; Claustre, H.; Bricaud, A.; Obolensky, G.; Hoepffner, N. Variations in the light absorption coefficients of phytoplankton, non-algal particles, and dissolved organic matter in coastal waters around Europe. *J. Geophys. Res.* **2003**, *108*, 4_1–4_20.
55. Fishwick, J.R.; Aiken, J.; Barlow, R.G.; Sessions, H.; Bernard, S.; Ras, J. Functional relationships and bio-optical properties derived from phytoplankton pigments, optical and photosynthetic parameters; a case study of the Benguela ecosystem. *J. Mar. Biol. Assoc. UK* **2006**, *86*, 1267–1280.
56. Hirata, T.; Aiken, J.; Hardman-Mountford, N.; Smyth, T.J.; Barlow, R.G. An absorption model to determine phytoplankton size classes from satellite ocean colour. *Remote Sens. Environ.* **2009**, *112*, 3153–3159.
57. Carder, K.L.; Cannizzaro, J.P.; Lee, Z. Ocean color algorithms in optically shallow waters: Limitation and improvements. *Proc. SPIE* **2005**, *5885*, doi:10.1117/12.615039.
58. Cannizzaro, J.P.; Carder, K.L. Estimating chlorophyll a concentration from remote-sensing reflectance in optically shallow waters. *Remote Sens. Environ*. **2006**, *101*, 13–24.
59. Aiken, J.; Pradhan, Y.; Barlow, R.G.; Lavender, S.; Poulton, A.; Holligan, P.M.; Hardman-Mountford, N. Phytoplankton pigments and functional types in the Atlantic Ocean: A decadal assessment, 1995–2005. *Deep-Sea Res. Part II: Top. Stud. Oceanogr.* **2009**, *56*, 899–917.
60. Cressie, N.A.C. *Statistics for Spatial Data*; John Wiley & Sons, Inc: New York, NY, USA, 1993; pp. 1–900.
61. Kanaroglou, P.S.; Soulakellis, N.A.; Sifakis, N.I. Improvement of satellite derived pollution maps with the use of a geostatistical interpolation method. *J. Geogr. Syst.* **2001**, *4*, 193–208.
62. Zhang, C.; Li, W.; Travis, D. Restoration of clouded pixels in multispectral remotely sensed imagery with co-kriging. *Int. J. Remote Sens.* **2009**, *30*, 2173–2195.
63. Meng, Q.; Borders, B.; Madden, M. High-resolution satellite image fusion using regression kriging. *Int. J. Remote Sens.* **2010**, *31*, 1857–1876.
64. Petrie, G.M.; Heasler, P.G.; Perry, E.M.; Thompson, S.E.; Daly, D.S. Inverse kriging to enhance spatial resolution of imagery. *Proc. SPIE* **2002**, *4789*, doi:10.1117/12.454822.
65. Wang, X.J.; Liu, R.M. Spatial analysis and eutrophication assessment for chlorophyll a in Taihu Lake. *Environ. Monit. Assess.* **2005**, *101*, 167–74.
66. Müller, D. Estimation of Algae Concentration in Cloud Covered Scenes Using Geostatistical Methods. In Proceeding of ENVISAT Symposium 2007, Montreux, Switzerland, 23–27 April 2007.

67. Georgakarakos, S.; Kitsiou, D. Mapping abundance distribution of small pelagic species applying hydroacoustics and Co-Kriging techniques. *Hydrobiologia* **2008**, *612*, 155–169.
68. Saulquin, B.; Gohin, F.; Garrello, R. Regional objective analysis for merging high-resolution MERIS, MODIS/Aqua, and SeaWiFS Chlorophyll-a data from 1998 to 2008 on the European Atlantic Shelf. *IEEE Trans. Geosci. Remote Sens.* **2010**, *49*, 143–154.
69. Shehhi, M.R.A.; Gherboudj, I.; Estima, J.; Ghedira, H. Geospatial Analysis of the Red-Tide over the Arabian Gulf. In Proceeding of the 1st Geospatial Scientific Summit, Dubai, United Arab Emirates, 12–13 November 2012.
70. Agrawal, G.; Sarup, J. Comparision of QUAC and FLAASH atmospheric correction modules on EO-1 Hyperion data of Sanchi. *Int. J. Adv. Eng. Sci. Technol.* **2011**, *4*, 178–186.
71. Simboura, N.; Panayotidis, P.; Papathanassiou, E. A synthesis of the biological quality elements for the implementation of the European Water Framework Directive in the Mediterranean ecoregion: The case of Saronikos Gulf. *Ecol. Indic.* **2005**, *5*, 253–266.
72. Morton, B.; Blackmore, G. South China Sea. *Mar. Pollut. Bull.* **2001**, *42*, 1236–1263.
73. Quangninh Province Statistics Office. *Quangninh. Statistical Yearbook 1955–2011*; Statistical Publishing House: Hanoi, Vietnam, 2012; pp.1–548.
74. Lihan, T.; Mustapha, M.A.; Rahim, S.A.; Saitoh, S.; Iida, K. Influence of river plume on variability of chlorophyll a concentration using satellite images. *J. Appl. Sci.* **2011**, *11*, 484–493.
75. CSTT (Comprehensive Study Task Team of Group Coordinating Sea Disposal Monitoring). *Comprehensive Studies for the Purposes of Article 6 & 8.5 of DIR 91/271 EEC, the Urban. Waste Water Treatment Directive*, 2nd ed.; The Scottish Environment Protection Agency and Water Service Association: Edinburgh, UK, 1997; pp. 8–11.
76. Cannizzaroa, J.P.; Cardera, K.L.; Chena, F.R.; Heilb, C.A.; Vargoa, G.A. A novel technique for detection of the toxic dinoflagellate, Kareniabrevis, in the Gulf of Mexico from remotely sensed ocean color data. *Cont. Shelf Res.* **2008**, *28*, 137–158.